Imaging Buried Archaeological Features through Ground Penetrating Radar: The Case of the Ancient Saepinum (Campobasso, Italy)

Marilena Cozzolino *, Vincenzo Gentile, Claudia Giordano and Paolo Mauriello

Department of Human, Social and Educational Science, University of Molise, Via De Sanctis, 86100 Campobasso, Italy; vincenzo.gentile86@gmail.com (V.G.); claudiagiordano12@hotmail.it (C.G.); mauriello@unimol.it (P.M.)
* Correspondence: marilena.cozzolino@unimol.it

Abstract: The archaeological area of Saepinum is considered the symbol of the history of Roman civilization in Molise region (Italy). It was a Samnite commercial forum and service center, then it became a Roman municipium, and, later, it was transformed into a medieval and modern rural village. Although the archaeological excavations brought to light different important public buildings, such as the theater, the forum, the basilica, different temples, and the main streets, today, there is still much to discover and study inside the well-preserved city walls. For this purpose, a ground penetrating radar (GPR) survey was realized in the space between the theater and the decumanus, allowing imaging of a complex regular pattern of archaeological features belonging to thermal buildings still buried in the soil.

Keywords: GPR; archaeological prospections; Saepinum; thermae

1. Introduction

The archaeological area of Saepinum (41°25′56.93″ N, 14°37′03.40″ E) is a plain center located at the base of the Matese Mountain that faces the Tammaro valley, in Molise Region in the northern zone of southern Italy [1] (Figure 1a).

The Roman city was preceded by a fortified center from the Samnite era (about 4th century B.C.) called Terravecchia di Sepino, which was conquered in 293 B.C. [2] during the third Samnite war [3,4]. Following this event, the center was abandoned and the population settled downstream at the intersection of two road axes, one at the bottom of the valley (today the Pescasseroli-Candela "tratturo", a transhumance route); the other, perpendicular to the latter, descends from the Matese and continues towards the hills of the Tammaro valley [5]. Consequently, the new center of Saepinum was built and the two road axes were incorporated in the city, becoming the decumanus (NW-SE main road) and the cardo (NNE-SSW main road) (Figure 1b,c).

The Roman city, which occupies an area of about 12 hectares, is delimited by city walls whose construction was realized in the period 2 B.C.–4 A.D. [6,7] (n. 2443). The circuit, which extends for a length of about 1270 m, was equipped with 19 circular towers (currently visible), arranged at a regular distance of about 25–30 m and four doors designed as triumphal arches, with a single vault. The doors were called Tammaro Gate (NNE side, in front of the Tammaro river's plain), Bovianum Gate (NW side, towards the city of Bojano), Beneventum Gate (SSW side, in the direction of the city of Benevento), and Terravecchia Gate (SSW side, towards the Matese Mountain) [8] (Figure 1b).
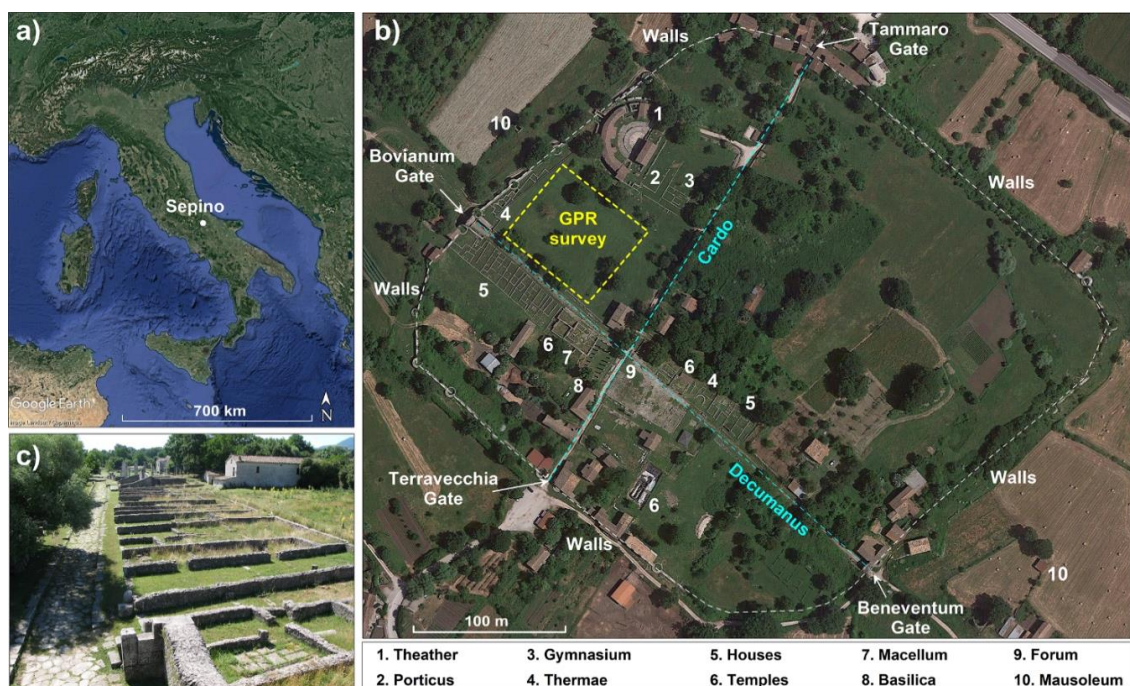
Figure 1. Location of Sepino on a Google Earth™ satellite image of Italy (**a**), map of the archaeological area of Saepinum with an indication of walls, main buildings, gates, and roads (**b**) and a picture of the decumanus flanked by private houses in a view from Bovaianum Gate in the direction of Beneventum Gate (**c**).

Archaeological excavations that began in the 1950s have brought to light only a small part of the Roman city. The archaeological analysis of the excavated and elevated structures has highlighted that the period of greatest splendor for Saepinum was the Augustan age, when the city took on significant urban growth due to the construction of the most important buildings [9]. In detail, the monumental structures actually found include (Figure 1b): The theater (1 in Figure 1b, Figure 2a) and the gymnasium-porticus complex (2 and 3 in Figure 1b) located in the northern sector of the city dated to the first half of the 1st century A.D.; the basilica located near the forensic area, built in the 1st century B.C. (8 in Figure 1b, Figure 2b); the macellum [10–12], the building used as a market, dated to the 1st century. A.D. [7] (n. 2475) (8 in Figure 1b); the cult buildings belonging to the 1st century A.D. and located on the decumanus, next to the macellum (7 in Figure 1b); the forum of the Augustan age located at the crossroads between the cardo and the decumanus (9 in Figure 1b); the thermal complex attached to the walls near Bovianum Gate dating back to 2nd century A.D. (4 in Figure 1b, Figure 2e); and the production buildings and the housing district located along the decumanus in the stretch between the forum and Beneventum Gate used since the Augustan age until the 5th century A.D. (5 in Figure 1b,c and Figure 2c).

Outside the wall circuit there are two necropolises, one near Bovianum Gate dated to the 1st century A.D. and the other of the Augustan age located outside Beneventum Gate [13] (10 in Figure 1b). Near the latter necropolis, archaeological excavations brought to light the remains of a medieval settlement dated to the 14th century.

In the 5th and 6th centuries A.D., the city was the diocesan office [14] but immediately lost importance due to the growing influence of the near city of Bojano, in the 9th century. Most of the population of Saepinum moved to a hill called Castellum Sepini [15], which later took the name of the actual Sepino. The name of Sepino appears in documents starting from the 12th century, but in that period, the city lost its greatness and it was reduced to a small village.

The interest in the archaeological history of Saepinum, as happened throughout the Molise territory, began in the mid-1800s. As evidenced by the rich current literature, many studies were carried

out up to now [8,16–26]. However, archaeological excavations concerned only 10% of the areas inside the walls.

The real need to increase the knowledge of the site, the impossibility of planning extensive excavations due to the large financial resources required, and the subsequent management for the conservation of the excavated structures have led to planning preventive non-invasive geophysical prospections in order to provide, in a fast way on vast areas, an image of archaeological features still buried in the soil. In this frame, different methods, such as electrical resistivity tomography, the magnetic method, the induced electromagnetic technique, and ground penetrating radar (GPR), are often employed with successful results [27–48].

In this work, the GPR technique was chosen for the survey because of the non-destructive features of the application, the high speed of data acquisition, and the optimal resolution of results. The main objective of the application was the production of a new detailed map of buried archaeological structures in an unexplored area located between the theater and the decumanus in the eastern part of the northern thermae (in yellow in Figure 1b). The gathered information, nonexistent so far, will be useful to plan the following actions of archaeological investigation, conservation and valorization of the area.

Figure 2. Pictures of the archaeological area of Saepinum: the theater (**a**), the basilica (**b**), the private houses (**c**) near Bovianum Gate (**d**), and the northeastern thermae (**e**).

2. Methods, Data Acquisition, and Processing

GPR is based on the diffusion of electromagnetic pulses into the soil and the recording of those re-radiated by buried targets, characterized by sufficient dimensions and by electromagnetic properties different from those of the receding ground. The quantities that are measured are the time required for the wave to travel the path from the transmitting antenna to a discontinuity and return to the surface (double time or two way time) and the amplitude of the reflected wave. The double travel time depends on the speed with which the wave propagates within the material and provides information on the depth at which the reflectors are located. The amplitude, however, which represents how much energy returns to the surface after reflection, depends on the initial energy of the sent wave, the quantity that it is dissipated along the way, and the contrast of the electromagnetic properties of the materials that determine the surface of the reflection. A complete description of the method is available in textbooks, such as [49–53].

The factors that influence the performance of the system, in terms of the detectability of existing targets, are the electromagnetic properties of the propagation medium, which determine the depth of investigation that can be reached, which therefore varies from point to point. Since the attenuation of

the means is a function of the radiated frequency, the use of low-frequency antennas generally allows extension of the penetration depth of the signals; however, this is at the expense of the resolution.

In this case, the RIS K2 Georadar (IDS GeoRadar s.r.l., Pisa, Italy), equipped with a multi-frequency TRMF (Time-Reversal Matched Filter) antenna (600–200 MHz), was used during data acquisition (Figure 3b). An area of about 10,700 m² was investigated through 342 profiles, NE-SW oriented, distributed on two bands overlapping by 1.5 m (Figure 3a). In practice, the two acquisition bands were divided into sub-cells with a maximum width of 20 m and a length of 27 m (western band) and 36 m (eastern band). The location of cell intersections was accurately measured through a total station using georeferenced fiduciary points for the absolute position. Profiles were spaced 0.5 m considering the total size of the investigation area and the investigative purposes, so as to achieve the detailed resolution most useful for data processing and their interpretation. Traverses were collected using a zig-zag collection mode in order to halve the acquisition times. Data acquisition was carried out in five days during the morning trying to work in the same soil moisture conditions in order to avoid an amplitude offset. Nevertheless, a variation over such a large period considering the broad dataset is inevitable.

Radar reflections on each line were recorded as 16-bit data in a time window of 90 ns, acquiring 512 samples per radar scan at 25 scans per mark (unit/marker, 1).
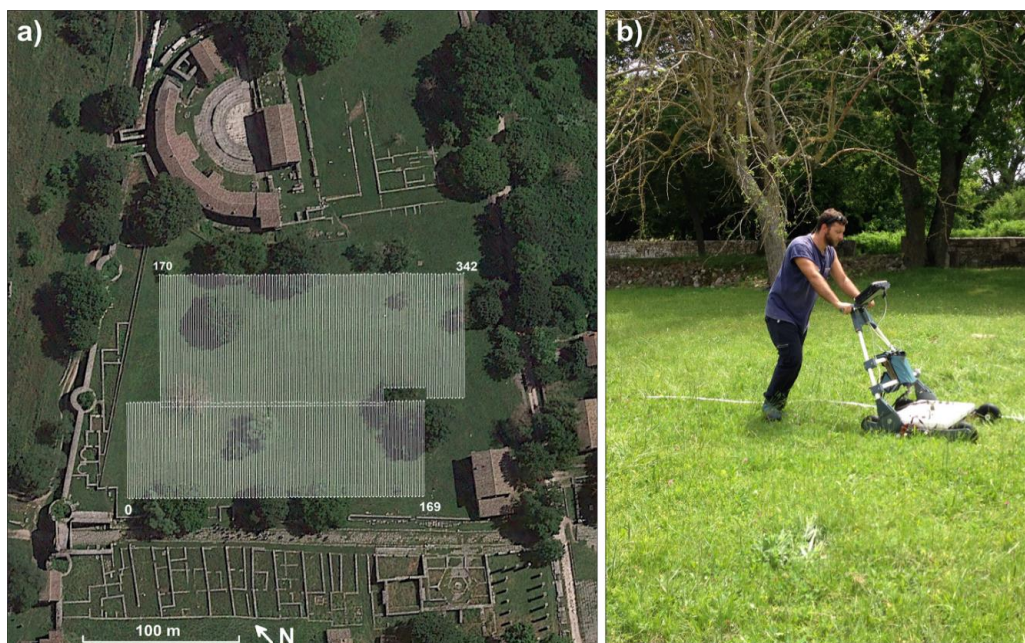
Figure 3. Grid data acquisition on a Google Earth™ satellite image (**a**) and the RIS K2 Georadar during the survey (**b**).

Raw data were processed using the IdsGred [54] and GPR−SLICE 7.0 software [55] using standard methodological approaches: Data and trace editing, subtraction of the dc-drift (wobble) in the data, time-zero correction matched considering the starting point of the wave (22) and the center frequency of 612 MHz, bandpass filter (low cutoff: 63 MHz; upper cutoff: 1252 MHz), background removal (the length of the filter was set to 1000 ensuring that the same average scan across the radargram is subtracted from every of the 512 scans as suggested in [55]), and automatic gain.

Finally, the whole data set was used to extract horizontal slices relative to different time windows equal to 4 ns with an overlap 1–2 ns. As the data set was so large and, as a consequence, the dielectric constant of the soil could be extremely variable, we avoided converting time to depth using a mean value with the possibility of obtaining an arbitrary and inaccurate estimate. Nevertheless, an average velocity of 100 m/mms was matched fitting some hyperbolas, that is, the expected buried feature is

very shallow, confined in the volume of soil included in the range 0.2–1.5 m. This evaluation is in agreement with the archaeological data considering that the excavated structures in the area appeared in the soil at few decimeters from the surface.

3. Results and Discussion

For brevity, examples of eight radargrams are reported in Figures 4 and 5, four for each band of acquisition. Here, circles and rectangles are used for the data interpretation using a different color for each radargram. The location of the circles on the top of the radargram represents the projection of deeper anomalies on the surface, a choice appositely made so as not to cover the section with graphic elements. The images put in evidence several punctual near-surface anomalies (marked with different colored circles) that are associated with possible targets stretched below the surface, such as foundations, walls, or channels, cut diagonally or transversely. Furthermore, great areas with sub-horizontal lying or highly disturbed bands is also evidence (indicated with colored rectangles), which is related to the septa of walls or collapsed areas with an accumulation of stones. All anomalies are located in the time window of 0–30 ns.
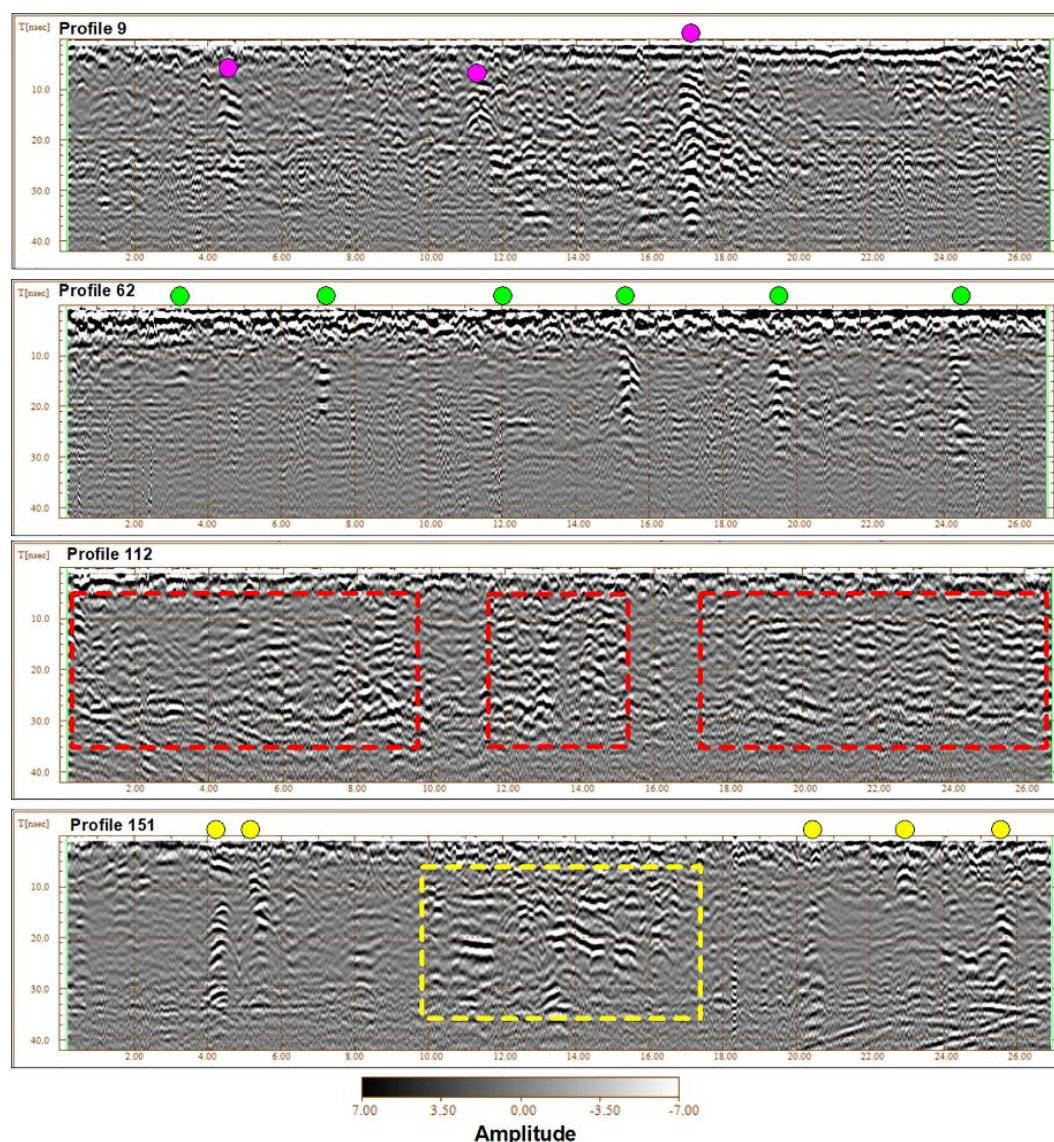
Figure 4. Radargrams 9, 62, 112, and 151 with an indication of the main anomalies.
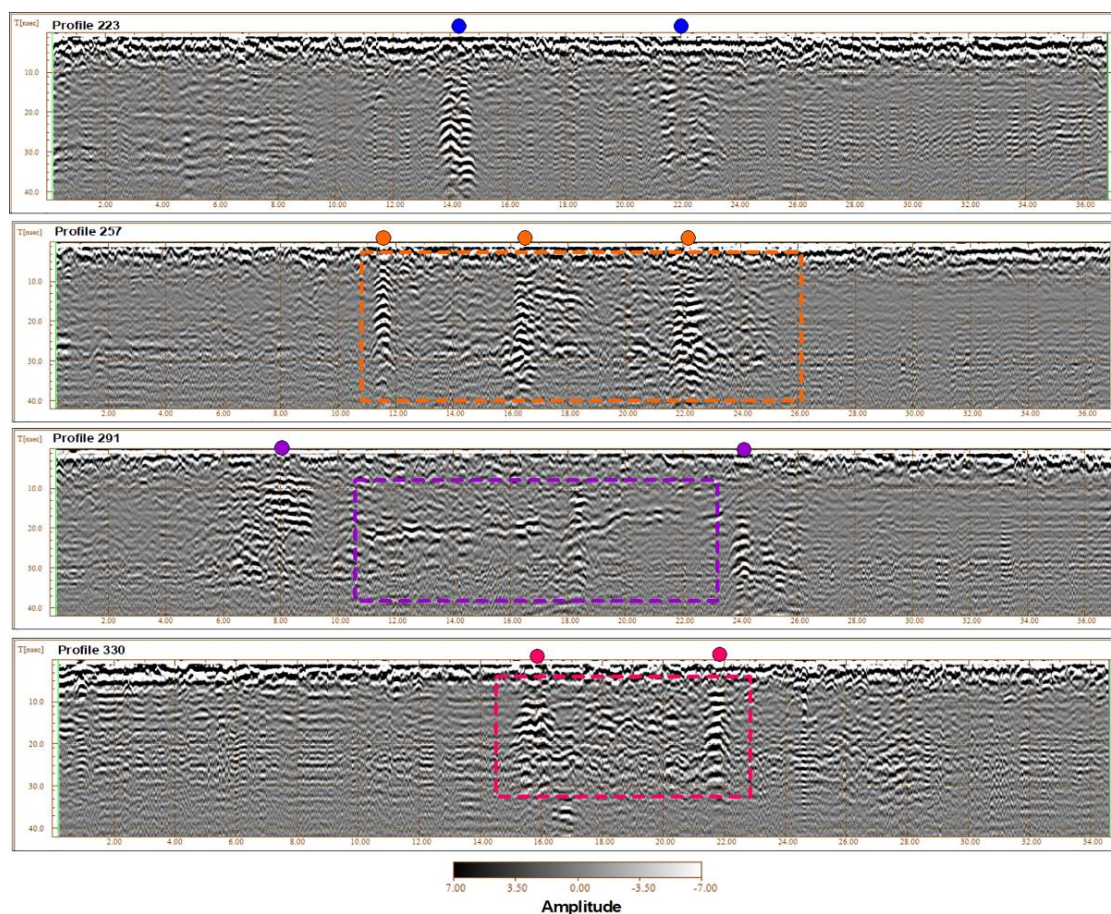
Figure 5. Radargrams 223, 257, 291, and 330 with an indication of the main anomalies.

The horizontal slices, better than vertical sections, allow recognition of a complex system of regular highs of the amplitude of the electromagnetic signals (Figure 6). Starting from the lowest to the highest time interval, an interesting intertwining of linear anomalies gradually emerges, which let to being able to imagine the presence of articulated buildings buried in the shallow subsoil. It is possible to recognize different types of alignments: Several parallel/perpendicular to the long side of the grid (NW-SE oriented as the decumanus) characterized by high values of the amplitude and different diagonals arrangements with medium measured values, almost intertwined with each other.

For an archaeological interpretation, the most significant slice related to 14–18 ns was taken into consideration. In Figure 7, a contour map is shown by applying the logarithmic scale to better represent the data set that extends over a very wide range of values and to highlight particular trends in the variation of the data.

Superimposed on the map (Figure 7), the locations of the eight analyzed radargrams are shown using the same graphics (circles and rectangles with the same color assignment) used in Figures 4 and 5 for the anomalies' interpretation. In this way, it is clear to understand how the colored point anomalies mentioned above are walls intercepted transversely and the horizontal anomalies are walls/collapses scanned along their entire length directly from the top surface.

The same map was correctly georeferenced and positioned on a Google Earth™ image, as shown in Figure 8. Here, it is possible to note that the supposed alignments are in accordance with the thermal system partially excavated to the north and with the private houses that are located west of the decumanus.

In Figure 9, an interpretation of the archaeological structures is attempted. It is possible to distinguish at least four groups of anomalies probably corresponding to as many separate buildings.
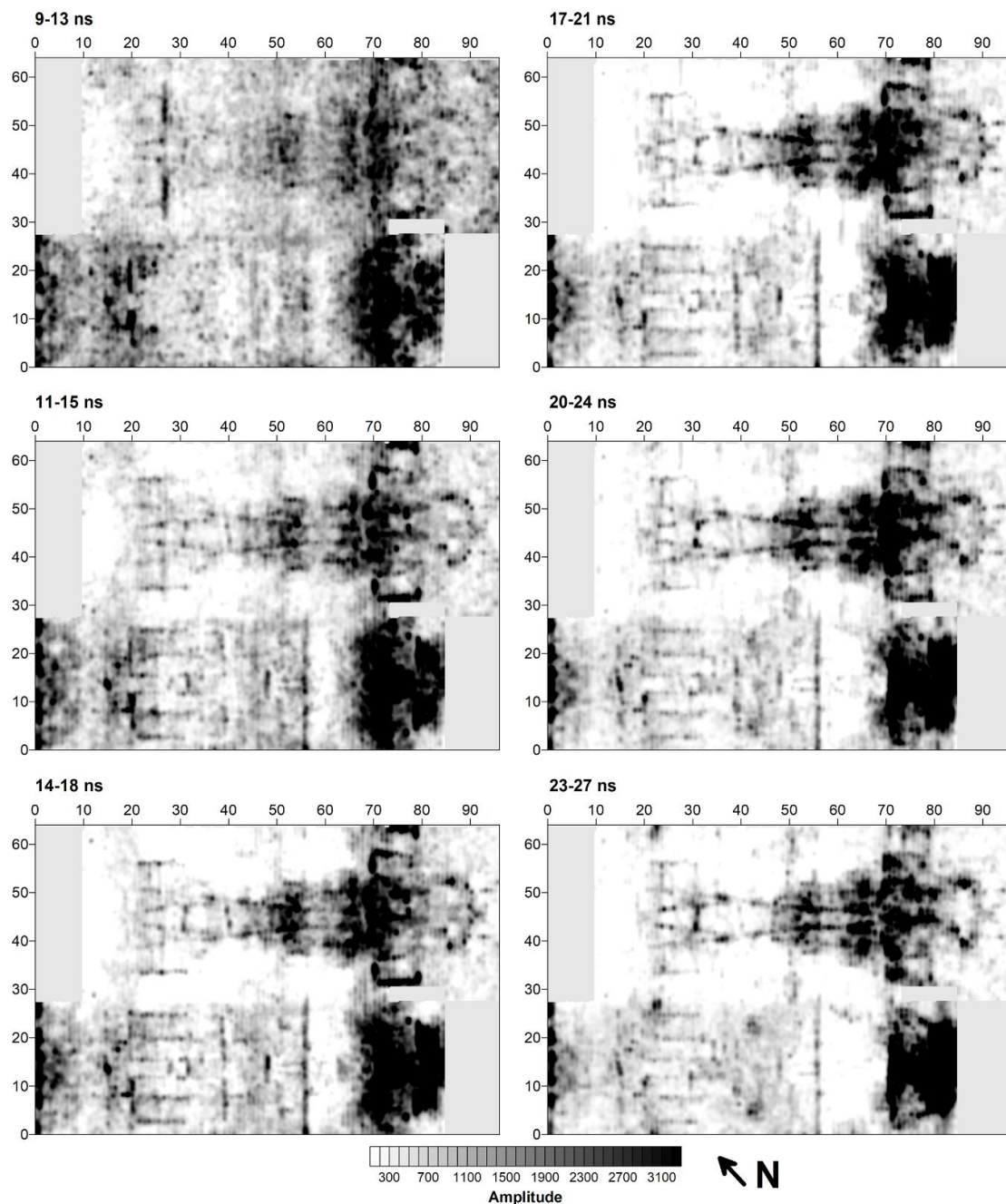
Figure 6. GPR time slices in the range 9–27 ns (distances in meters).

A first group, interpreted with magenta lines, represents the probable closure of the thermal complex that is located north of a wall partition about 28 m long. It is bordered to the south by a semi-circular structure with a diameter of about 12 m in the center (1 in Figure 9) and two rooms (4 m × 4 m) at the sides.

Moving to south, a second articulated building (marked with green lines) is hypothesized. The overall size of the anomalies is about 24 m × 56 m. In particular, a structure is supposed that is symmetrical with respect to the NE-SW-oriented center, characterized by two specular semicircles (diameter of 12 m similar to the previous one, 2 and 3 in Figure 9). In the center, on the line of symmetry, there is a square anomaly (4 in Figure 9) flanked on the sides by two rooms 10 m long and 4 m wide (5 and 6 in Figure 9). On the southern side, an alignment 30 m long, bordered by two cells of equal size (4 m × 4 m) at the ends (7 and 8 in Figure 9), closes the complex.

The third anomaly is located in front of the temple, which is located west of the decumanus and has dimensions of 26 m × 14 m (indicated in blue, 9 in Figure 9). Inside, it is possible to recognize orthogonal divisions between them.

The fourth group has considerable dimensions of 70 m × 22 m (in red in Figure 9). The complex is symmetrical with respect to the NE-SW-oriented center and several regular patterns can be identified. From north to south, the following features are highlighted:

- Three cells (10 in Figure 9) flanked by two single alignments that close orthogonally with two septa;
- A 10 m × 10 m square anomaly (11 in Figure 9);
- Five cells of which the central one is slightly larger and bordered to the north from an open room (12 in Figure 9);
- Regular and symmetrical segments (13 in Figure 9);
- A complex with articulated internal divisions bordered by two large lateral rooms (14 and 15 in Figure 9); and
- A semicircular anomaly of similar dimensions to the previous discussed (16 in Figure 9).

In addition, analyzing the completely horizontal slices, oblique anomalies are interpreted (Figure 10). They are regularly distributed, in some cases symmetrical, and often connect anomalies, with different orientations just discussed in the corners.
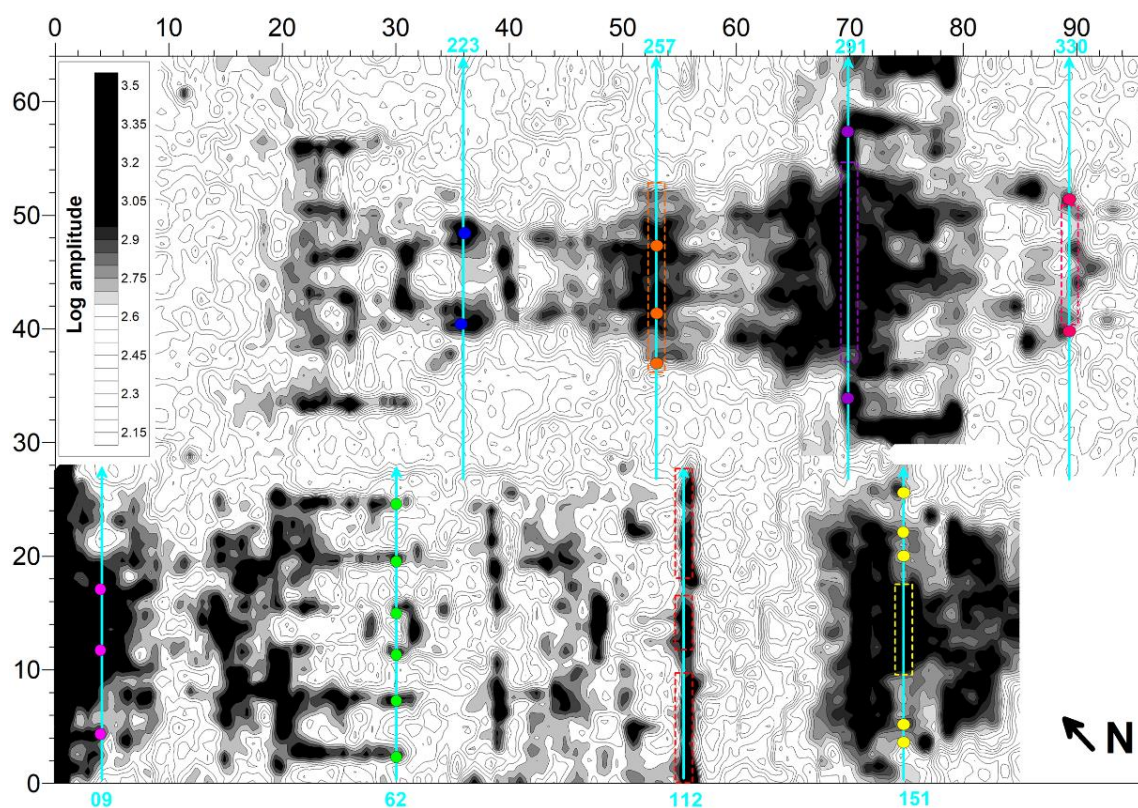
Figure 7. Time slice relative to 14–18 ns with the location and the interpretation of the eight radargrams reported in Figures 4 and 5 (distances in meters).

Figure 8. Time slice relative to 14–18 ns overlapped to a Google Earth™ satellite image.
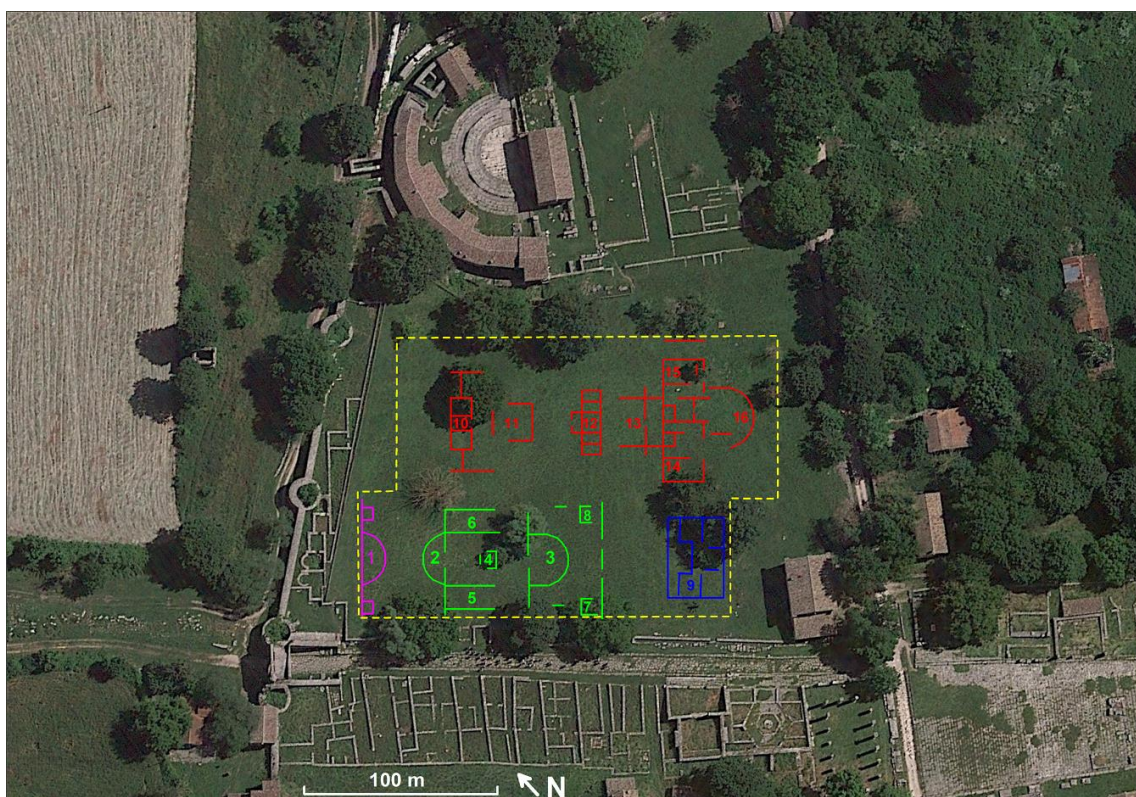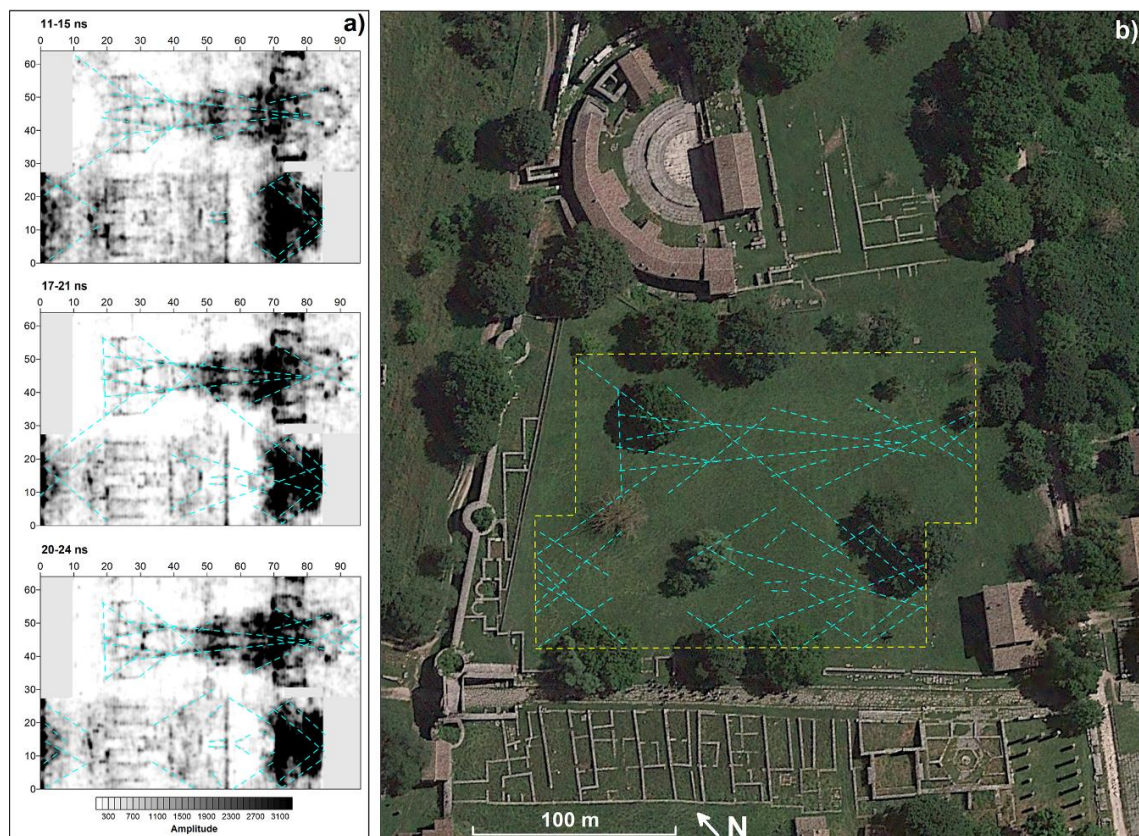

Figure 9. Interpretation lines reported on a Google Earth™ satellite image.

Figure 10. Oblique anomalies on selected time slices (**a**) and interpretation lines reported on a Google Earth™ satellite image (**b**).

4. Conclusions

The GPR investigations conducted in the ancient city of Saepinum provided important information about the imaging of archaeological structures still buried in the subsoil.

Given the articulation of the anomalies and their geometric characteristics enriched with apsidal environments, it can be assumed that they belong to a thermal complex. This allowed us to fully define this type of construction, which was partially excavated in this sector to date.

Particularly clear are the contours of the four identified buildings or building complexes. The first represents the closure of what is visible today in the thermae; the second, with the two apsed rooms and the various environments identified, represents a novelty in the knowledge of the site; the third, of dubious function, has very regular features; and the fourth, of imposing size, has the clear constructive characteristics of the thermae. The latter, similar to the known thermae (for example, those of Domu'e Cubas, Sardinia, Italy), could be composed from south to north by a changing room (apodyterium), a cold environment (frigidarium), a warm environment (tepidarium), a warm room (calidarium), and a laconicum (room with hot air) with praefurnium (oven) and suspensurae.

In this context, the numerous oblique anomalies intercepted are justified and thus can be interpreted as small channels for the supply of water to the various rooms.

The results presented, in addition to enriching the knowledge of the site by increasing the percentage of surface studied so far, have contributed to confirming the great wealth that the city had until the 4th century A.D. [8] (Figure 11). Furthermore, it can be considered a valid and useful example of geophysical investigations for archeology available to scientists and local/national decision makers that operate in the frame of cultural heritage protection for planning future activities.
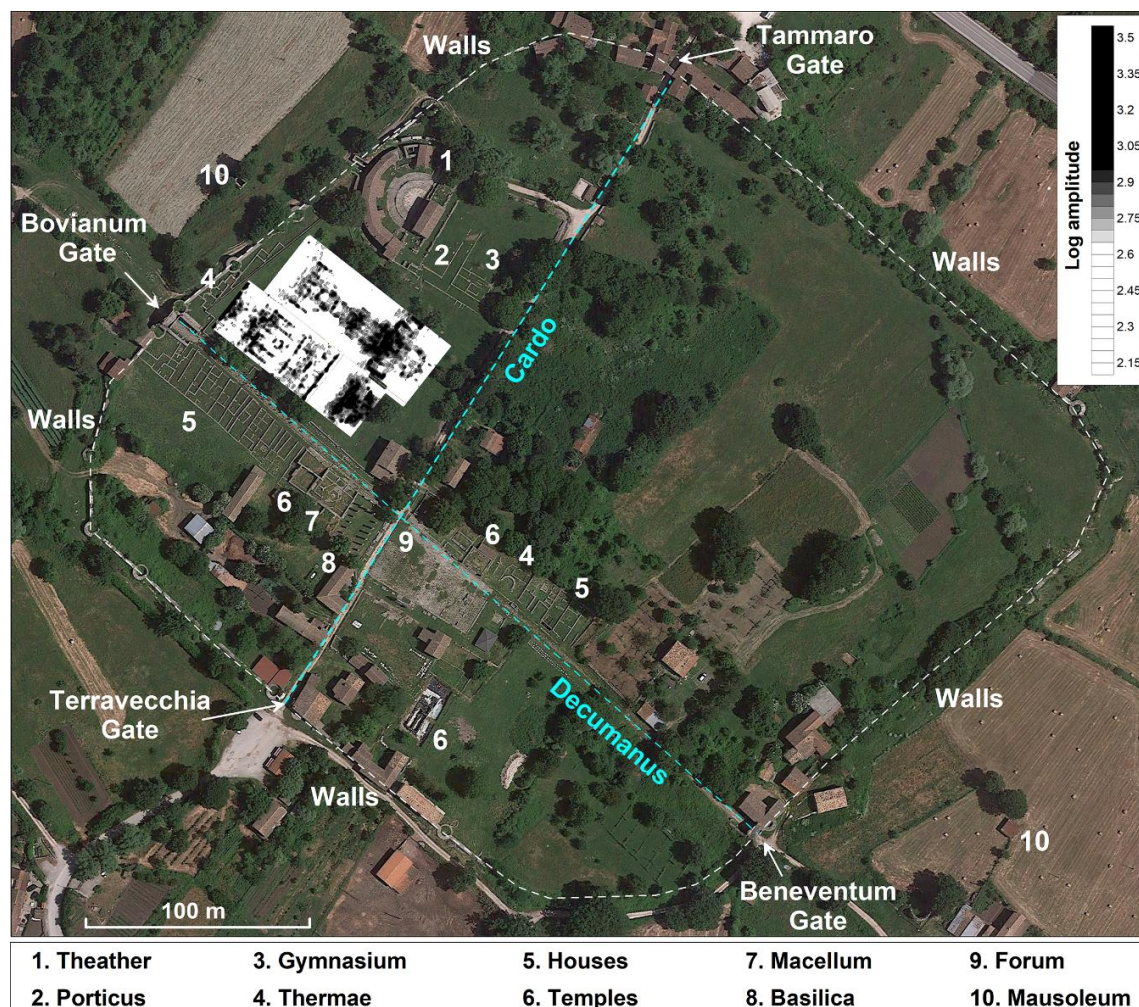
Figure 11. Uploaded archaeological map of the ancient Saepinum with the addition of the time slice relative to 14–18 ns.

As the results look to be so promising, future field campaigns of prospection are planned using the area as a test site, where the following parameters of acquisition will be varied: The frequency of the antennas and the spacing between profiles with a minor interline, as well as integrating the GPR measurements with magnetometry, resistivity tomography, and induce electromagnetic methods. The aim is to define the limits and advantages and to set a protocol of best settings for each method when studying a real case. Anyway, the research is still ongoing, and the project regards the prospection of all free areas inside the city walls.

Conflicts of Interest: The authors declare no conflict of interest.

References

1. Valente, E.; Cozzolino, M. GIS mapping of the archaeological sites in the Molise region (Italy). *Archeol. Calc.* **2019**, *30*, 367–385.

2. Oakley, S.P. The Tammaro Valley. In *The Hill-Forts of the Samnites*; British School at Rome: Rome, Italy, 1995; pp. 69–72.

3. Titi Livi. *Ab Urbe Condita, X, 45, 12*; Oxford University Press: Oxford, UK, 1955.

4. La Regina, A.I. Sanniti. In *Italia Omnium Terrarum Parens*; Libri Scheiwiller: Milan, Italy, 1989; pp. 301–342.

5. Ceccarelli, A.; Fratianni, G. I centri sannitici: Sepino. In *Archeologia delle Regioni di Italia Molise*; BraDypUS: Rome, Italy, 2017; pp. 150–153.

6. Pinder, I. Saepinum: The Augustan walls and their urban context. *Consid. Stor. Archeol.* **2016**, *9*, 21–42.

7. Mommsen, T. *Corpus Inscriptionum Latinarum IX Inscriptiones Calabriae, Apuliae, Samnii, Sabinorum Piceni Latinae*; n. 2443; G. Reimer: Berlin, Germany, 1883.

8. De Benedittis, G.; Gaggiotti, M.; Matteini Chiari, M. *Saepinum: Sepino*; Tipolitografia Fotolampo: Campobasso, Italy, 1993.

9. Romano, G. Saepinum. *Forma Urbis* **2006**, *9*, 4–12.

10. De Ruyt, C.; Mertens, J. *Macellum: Marché alimentaire des Romains*; Louvain-La-Neuve: Walloon Brabant, Belgium, 1983.

11. De Ruyt, C. Exigences fonctionnelles et variété des interpretations dans l'architecture des macella du monde romain. In Proceedings of the Mercati permanenti e Mercati periodici del mondo romano, Capri, Italy, 13–15 October 1997; Lo Cascio, E., Ed.; Edipuglia: Bari, Italy, 2000; pp. 177–186.

12. De Ruyt, C. Les produits vendu à macellum. In *Sacrifices, Marché de la Viande et Pratiques Alimentaires dans les Cites du Monde Romain*; Van Andringa, W., Ed.; Brepols: Turnhout, Belgium, 2008; pp. 135–150.

13. Soricelli, G. Le forme municipali in Italia e nelle province occidentali tra i secoli I a.C. e III d.C. In Proceedings of the Atti della XXI Rencontre franco-italienne sur l'épigraphie du monde romain, Campobasso, Italy, 24–26 September 2015; Evangelisti, S., Ricci, C., Eds.; Edipuglia: Bari, Italy, 2017; pp. 89–102.

14. Catalano, D. Il Molise medievale tra perdite, trasformazioni e decontestualizzazioni. In *Il Molise Medievale. Archeologia e arte*; Ebanista, C., Monciatti, A., Eds.; All'Insegna Del Giglio: Florence, Italy, 2010; pp. 175–189.

15. Gaggiotti, M.; De Benedittis, G. Da Saepinum al Castellum Sepini. *AIM* **1986**, *II*, 133–139.

16. Iasello, I.M. *Samnium: Assetti e trasformazioni di una provincia dell'Italia tardoantica*; Edipuglia: Bari, Italy, 2007.

17. Cianfarani, V. Sepino, teatro: Campagna di scavo 1950. *Not. Scav.* **1950**, *1951*, 88–106.

18. Cianfarani, V. *Saepinum*; Soprintendenza alle antichità degli Abruzzi e del Molise: Chieti, Italy, 1954.

19. Cianfarani, V. *Guida alle antichità di Sepino*; Pleion: Milan, Italy, 1958.

20. Cianfarani, V. Vecchie e nuove iscrizioni sepinati. In Proceedings of the Atti del III Congresso Internazionale di Epigrafia Greca e Latina, Rome, Italy, 4–8 September 1957; L'ERMA di Bretschneider: Rome, Italy, 1959; pp. 371–380.

21. Matteini Chiari, M. «Il territorio in età preromana», Il periodo preromano, Il lato corto sud est del foro. In *Saepinum: Sepino*; Tipolitografia Fotolampo: Campobasso, Italy, 1979; pp. 5–6, 18–19, 97–100.

22. Matteini Chiari, M. Il sepolcreto altomedievale dell'area forense di Sepino. In *La Necropoli di Vicenne Nella Piana di Bojano. Il Sannio tra Tardo Impero ed alto Medioevo*; La Rapida Grafedit: Matrice, Italy, 1988; pp. 9–94.

23. Matteini Chiari, M. Saepinum tra evo antico e medioevo. Nuove preliminari acquisizioni dal cantiere di scavo di San Pietro di Cantoni di Sepino. In Proceedings of the Atti del Convegno Internazionale di Studi "I Beni Culturali del Molise. Il Medioevo", Campobasso, Italy, 18–20 November 1999; pp. 184–198.

24. Matteini Chiari, M. (Ed.) *Saepinum, Museo documentario dell'Altilia*; La Rapida Grafedit: Matrice, Italy, 1982.

25. De Benedittis, G. *Echi del Sannio: Guida alle Antichità di Saepinum*; Tipolitografia Fotolampo: Campobasso, Italy, 2015.

26. Ceglia, V. Sepino-Altilia (CB) – Il Sistema idrico e fognante. *Consid. Stor. Archeol.* **2015**, *8*, 23–32.

27. Tsokas, G.N.; Sarris, A.; Pappa, M.; Bessios, M.; Papazachos, C.B.; Tsourlos, P.; Giannopoulos, A. A large scale magnetic survey in Makrygialos (Pieria), Greece. *Archaeol. Prospect.* **1997**, *4*, 123–137. [CrossRef]

28. Godio, A.; Sambuelli, L.; Socco, L.V. Electromagnetic survey for detection of archaeological remains in urban sites. *Lead. Edge* **2000**, *19*, 850–854. [CrossRef]

29. Maillol, J.; Ciobotaru, D.; Moravetz, I. Electrical and magnetic response of archaeological features at the early Neolithic site of Movila lui Deciov, western Romania. *Archaeol. Prospect.* **2004**, *11*, 213–226. [CrossRef]

30.　Vafidis, A.; Economou, N.; Ganiatsos, Y.; Manakou, M.; Poulioudis, G.; Sourlas, G.; Vrontaki, E.; Sarris, A.; Guy, M.; Kalpaxis, T. Integrated geophysical studies at ancient Itanos (Greece). *J. Archaeol. Sci.* **2005**, *32*, 1023–1036. [CrossRef]

31.　Ekinci, Y.L.; Kaya, M.A. 3D resistivity imaging of buried tombs at the Parion necropolis (NW Turkey). *J. Balk. Geophys. Soc.* **2007**, *10*, 1–8.

32.　Drahor, M.G.; Kurtulmuş, T.Ö.; Berge, M.A.; Hartmann, M.; Speidel, M.A. Magnetic imaging and electrical resistivity tomography studies in a Roman military installation found in Satala archaeological site, northeastern Anatolia, Turkey. *J. Archaeol. Sci.* **2008**, *35*, 259–271. [CrossRef]

33.　Berard, B.A.; Maillol, J.M. Common-and multi-offset ground-penetrating radar study of a Roman villa, Tourega, Portugal. *Archaeol. Prospect.* **2008**, *15*, 32–46. [CrossRef]

34.　Keay, S.; Earl, G.; Hay, S.; Kay, S.; Ogden, J.; Strutti, K.D. The role of integrated geophysical survey methods in the assessment of archaeological landscapes: The case of Portus. *Archaeol. Prospect.* **2009**, *16*, 154–169. [CrossRef]

35.　Udphuay, S.; Paul, V.L.; Everett, M.E.; Warden, R.B. Ground penetrating radar imaging of Twelfth Century Romanesque foundations beneath the Thirteenth Century Gothic Abbey Church of Valmagne, France. *Archaeol. Prospect.* **2010**, *17*, 199–212. [CrossRef]

36.　Pincus, J.A.; de Smet, T.S.; Tepper, Y.; Adams, M.J. Ground-penetrating radar and electromagnetic archaeogeophysical investigations at the Roman Legionary Camp at Legio, Israel. *Archaeol. Prospect.* **2013**, *20*, 175–188. [CrossRef]

37.　Neubauer, W.C.; Gugl, M.; Scholz, G.; Verhoeven, I.; Trinks, K.; Löcker, M.; Doneus, T.; Van Meirvenne, M. The discovery of the school of gladiators at Carnuntum, Austria. *Antiquity* **2014**, *88*, 173–190. [CrossRef]

38.　Urban, T.M.; Leon, J.F.; Manning, S.W.; Fisher, K.D. High resolution GPR mapping of late bronze age architecture at Kalavasos-Ayios Dhimitrios, Cyprus. *J. Appl. Geophys.* **2014**, *107*, 129–136. [CrossRef]

39.　Amato, V.; Cozzolino, M.; De Benedittis, G.; Di Paola, G.; Gentile, V.; Giordano, C.; Marino, P.; Rosskopf, C.M.; Valente, E. An integrated quantitative approach to assess the archaeological heritage in highly anthropized areas: The case study of Aesernia (southern Italy). *IMEKO* **2016**, *5*, 33–43. [CrossRef]

40.　Ranieri, G.A.; Godio, F.; Loddo, S.; Stocco, A.; Casas, P.; Messina, P.; Orfila, M.; Cau, M.A.; Chaves, M.E. 2016 Geophysical prospection of the roman city of pollentia, alcudia (Mallorca, baleric island, spain). *J. Appl. Geophys.* **2016**, *134*, 125–135. [CrossRef]

41.　Fernández-Álvarez, J.P.; Rubio-Melendi, D.; Castillo, J.A.Q.; González-Quirós, A.; Cimadevilla-Fuente, D. Combined GPR and ERT exploratory geophysical survey of the Medieval Village of Pancorbo Castle (Burgos, Spain). *J. Appl. Geophys.* **2017**, *144*, 86–93. [CrossRef]

42.　Küçükdemirci, M.; Özer, E.; Piro, S.; Baydemir, N.; Zamuner, D. An application of integration approaches for archaeo-geophysical data: Case study from Aizanoi. *Archaeol. Prospect.* **2017**, 1–12. [CrossRef]

43.　Balkaya, Ç.; Kalyoncuoğlu, Ü.Y.; Özhanlı, M.; Merter, G.; Çakmak, O.; Talih Güven, I. Ground-penetrating radar and electrical resistivity tomography studies in the biblical Pisidian Antioch city, southwest Anatolia. *Archaeol. Prospect.* **2018**, *25*, 285–300. [CrossRef]

44.　Deiana, R.; Bonetto, J.; Mazzariol, A. Integrated electrical resistivity tomography and ground penetrating radar measurements applied to tomb detection. *Surv. Geophys.* **2018**, *39*, 1081–1105. [CrossRef]

45.　Cozzolino, M.; Longo, F.; Pizzano, N.; Rizzo, M.L.; Voza, O.; Amato, V. Multidisciplinary Approach to the Study of the Temple of Athena in Poseidonia-Paestum (Southern Italy): New Geomorphological, Geophysical and Archaeological Data. *Geosciences* **2019**, *9*, 324. [CrossRef]

46.　de Smet, T.S.; Everett, M.E.; Warden, R.R.; Komas, T.; Hagin, J.N.; Gavette, P.; Martini, J.A.; Barker, L. Fate of the historic fortifications at Alcatraz island based on virtual ground-testing of ground-penetrating radar interpretations from the recreation yard. *Near -Surf. Geophys.* **2019**, *17*, 151–168. [CrossRef]

47.　Cozzolino, M.; Caliò, L.M.; Gentile, V.; Mauriello, P.; Di Meo, A. The Discovery of the Theater of Akragas (Valley of Temples, Agrigento, Italy): An Archaeological Confirmation of the Supposed Buried Structures from a Geophysical Survey. *Geoscience* **2020**, *10*, 161. [CrossRef]

48.　Cozzolino, M.; Baković, M.; Borovinić, N.; Galli, G.; Gentile, V.; Jabučanin, M.; Mauriello, P.; Merola, P.; Živanović, M. The contribution of geophysics to the knowledge of the hidden archaeological heritage of Montenegro. *Geoscience* **2020**, *10*, 5. [CrossRef]

49.　Conyers, L.B. *Interpreting Ground-Penetrating Radar for Archaeology*; Left Coast Press: Walnut Creek, CA, USA, 2012.

50. Everett, M.E. *Near-Surface Applied Geophysics*; Cambridge University Press: Cambridge, UK, 2013.

51. Goodman, D.; Piro, S. *GPR Remote Sensing in Archaeology*; Springer: Heidelberg, Germany, 2013.

52. Reynolds, J.M. *2011 An Introduction to Applied and Environmental Geophysics*, 2nd ed.; John Wiley & Sons: Oxford, UK, 2011.

53. Cozzolino, M.; Di Giovanni, E.; Mauriello, P.; Piro, S.; Zamuner, D. *Geophysical Methods for Cultural Heritage Management*; Springer Geophysics Series: Cham, Switzerland, 2018.

54. Ground Penetrating Radar, Products. Available online: www.idsgeoradar.com (accessed on 24 April 2020).

55. Goodman, D. *GPR-SLICE. Ground Penetrating Radar Imaging Software. User's Manual*; Geophysical 629 Archaeometry Laboratory: Los Angeles, CA, USA, 2004.